NAL TR-970T

ISSN 0389-4010
UDC 621.438
532.5

TECHNICAL REPORT OF NATIONAL AEROSPACE LABORATORY

TR-970T

Mechanisms of Secondary Flows and Losses within a Three Dimensional Turbine Stator Cascade

A. YAMAMOTO, R. YANAGI and H. NOUSE

April 1988

NATIONAL AEROSPACE LABORATORY

CHŌFU, TOKYO, JAPAN

Mechanisms of Secondary Flows and Losses within a Three Dimensional Turbine Stator Cascade*

Atsumasa YAMAMOTO,** Ryoji YANAGI,**
and Hiroyuki NOUSE**

ABSTRACT

In order to reveal aerodynamic loss mechanisms of turbine blade rows, internal flows of a low-speed three-dimensional tubine stator cascade were measured in detail using five-hole pitot tubes. Flow visualization tests and the cascade endwall static-pressure measurements were also made. These test results show that many vortical flows relate to the loss generation but the major process of loss generation in the cascade passage can be explained simply as a migration process in which boundary layer fluids with low energy being developed on the cascade passage walls (i.e., both endwalls and both blade surfaces) migrate onto the blade suction surface near the trailing edge. Complicated flow patterns were seen rather in the vortical flows near the trailing edge and downstream of the cascade: for example, a strong trailing-shedding-vortex occurring downstream of the cascade affects the upstream flow field within the cascade by extremely complicated mechanisms. Effects of blade tip leakage flow on the cascade internal flow and the associated loss are also shown in this paper.

概　　要

タービン翼列の空力損失の発生メカニズムを明らかにするために，低速三次元タービン静翼列の内部流を5孔ピトー管を用いて詳細に測定した。同時に流れの可視化試験および翼列のエンドウォールの静圧測定も行った。その結果，翼列損失は多くの渦流に関与しているが，翼間での損失の主要発生過程は単に翼列流路壁（両エンドウォールおよび翼面表面）上で発達した低エネルギーの境界層流体が翼後縁近傍で翼負圧面上に移動する過程と説明できる。複雑な流れ模様はむしろ翼列下流および翼後縁近傍の渦流の内に見られ，たとえば翼列下流で発生する強い後縁はくり渦は上流の翼列内流れ場に非常に複雑なメカニズムで影響を与えている。翼列内部流及び損失に及ぼす翼先端漏れ流れの影響の結果についても示した。

NOMENCLATURE

CPs	:	Dimensionless static pressure
CPt	:	Total pressure loss coeficient
CVm	:	Dimensionless velocity
Ps	:	Static pressure
Pt	:	Total pressure
Vm	:	Flow velocity measured
Vs	:	Magnitude of secondary flow vector
Δ	:	Interval of contour plot
φ	:	Inclined angle of pitot tube against radial direction

* Received 27 February, 1988
** Aeroengine Division

ρ : Specific weight
θp : Pitch flow angle
1–5 : Indicate no. of traverse measurement planes
= : Indicates mass-averaged value

INTRODUCTION

Recent advanced technologies for high-efficiency gas turbine engines require accurate and detailed knowledge of flow mechanisms occuring within the turbomachinery in order to reduce losses. Reliable knowledge is required of complex three dimensional internal flows of advanced thick, high-turning-angle blade rows suitable for high temperature turbines using cooling. It is also necessary to know how performance is affected by coolant injected from the blades and leaking from the hub/tip walls. A lot of data on three dimensional flows of annular blade rows have been presented in the past. Detailed experimental measurements of the flow field within annular blade rows, however, have been limited; e.g., Sjolander [1], Bindon [2] and Sieverding et al. [3]. Of these, only Sieverding et al. [3] made detailed quantitative measurements of secondary flow vectors within a stator row, using double-head four-hole pitot tubes. Representation of secondary flow vectors makes the flow mechanism easily understandable. A work by Langston et al. [4] makes a good reference on such inter-blade flow measurements, although it is on a plane rotor cascade.

Over 300 tests, including flow visualization tests, were conducted at NAL in a serial study of coolant effects on turbine performance. In these tests, detailed traverse measurements were made in eleven measuring planes located in and out of the stator blade row of a low-speed annular air-cooled single-stage turbine. This serial study included tests with and without coolant injection from the blades and from the hub casing, with/without tip-clearance, and with/without the rotor installed. Over two million bits of accurate and detailed pressure data on secondary flows and total pressure losses were obtained using a fully automatic measurement system. Some of the results have already been presented by the authors et al. [5, 6].

In the present paper, efforts are concentrated on analyzing a mechanism for production and development of secondary flows and total pressure losses occuring within a stator blade row without coolant injection. The analysis is facilitated by the fact that a considerable quantity of computer graphics which clearly present the mechanism, were obtained from the experimental data. A complete set of test data is included in the paper also for future comparison with numerical analyses.

EXPERIMENTAL FACILITIES AND TEST PROGRAM

Details of the present test facilities have been given by the authors elsewhere [6].

Low-Speed Annular Turbine Stator Row

The test rig used (Fig. 1) is a suction-type wind tunnel which the author (A.Y.) designed for detailed studies of internal flows in annular turbine cascades. In the present tests, rotor blades were not installed.

The stator blades are untwisted, with a constant profile from hub to tip. The blades are bolted on an annular hub wall so that the lines of the blade trailing edges are normal to the wind tunnel center axis. This is the same method as that adopted by Sjolander [1]. The blade leading-edge lines of the present row are inclined against the radial direction of the wind tunnel. The blade profile, cut by a cylindrical surface at the mean blade span, is the same as the 'Mean' profile of one of NAL's high tempereature turbines for aeroengine use [7], and is also the same as that reported by Whitney et al. [8]. The present cascade is characterized by a high-turning angle, thick leading and trailing edges, low aspect ratio,

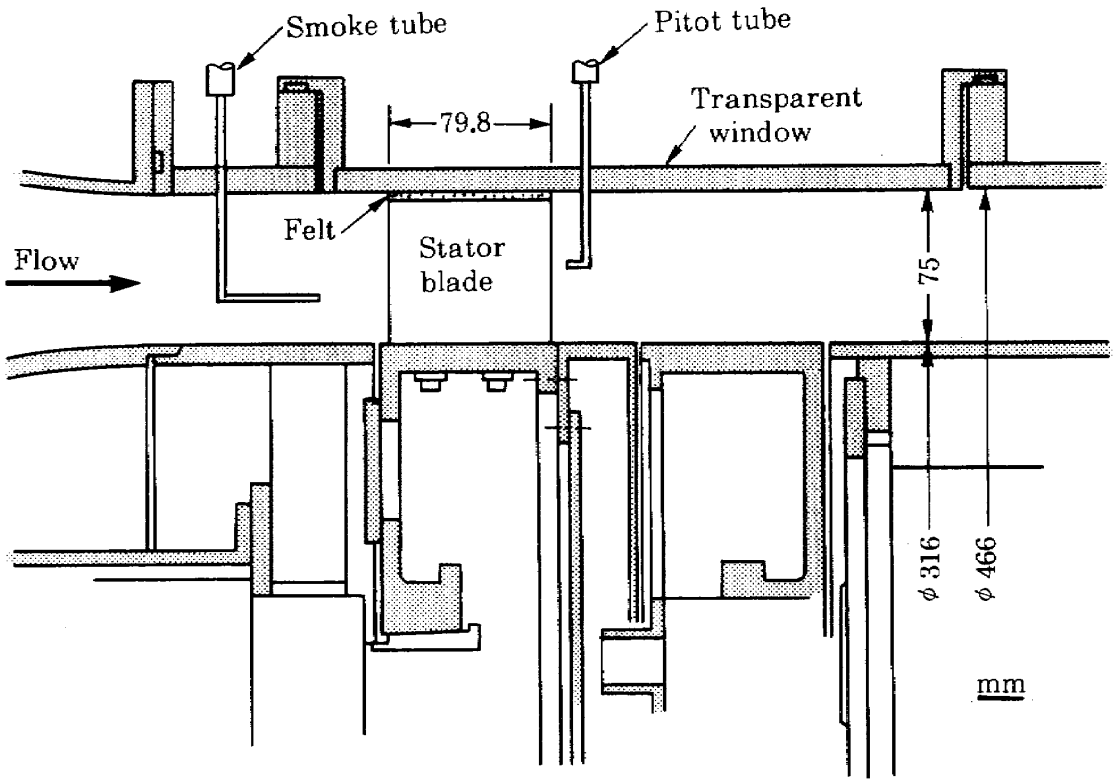

Fig. 1 Test section of NAL low speed turbine

low solidity, and low hub-to-tip radius ratio. The upper half casing of the test section has a 300mm, half cylindrical, transparent plexiglass window to allow inspection of the stator and rotor rows. Major specifications of the present test vane are shown in Table 1.

The stator row is rotatable by a pulse motor drive through a harmonic (planetary) reduction gear. This is for ease in making the circumferential traverse measurements. Blade tip clearance was sealed by felt material. In some tests with tip clearance of about 1%, this sealing was removed.

Table 1 Major stator specifications

Hub diameter, d_h	0.316 m
Hub-to-tip dia. ratio, d_h/d_t	0.68
Blade chord (manufactured), c	0.104 m
Aspect ratio, h/c	0.72
Solidity at mean, s/c	0.59
Stagger angle, ξ	39°
Design inlet flow angle, α_1	0°
Design outlet flow angle, α_2	66°

Test Conditions and Programs

Inlet flow condition was set by a Prandtl-type total/static pressure probe fixed at a mean radius position upstream from the cascade. The inlet flow velocity was kept constant for all traverse measurements. The cascade flow Reynolds number, based on mean outlet flow velocity and the blade chord, is about 2.4×10^5.

Traverse measurements were made with programmable three-axis NC controllers for pulse motor drives connected to a micro computer. Mechanical resolution of the devices is 0.045mm for the radial traverse and 1/200 degree for the circumferential. The accuracy of positioning of the sensors is about the same as the resolution.

Six measuring planes analyzed in the paper are shown in Figs. 2 and 3. The axial distances, measured from the blade leading edge, of planes 1, 2, 3, 4', 4 and 5 are -19mm (upstream the

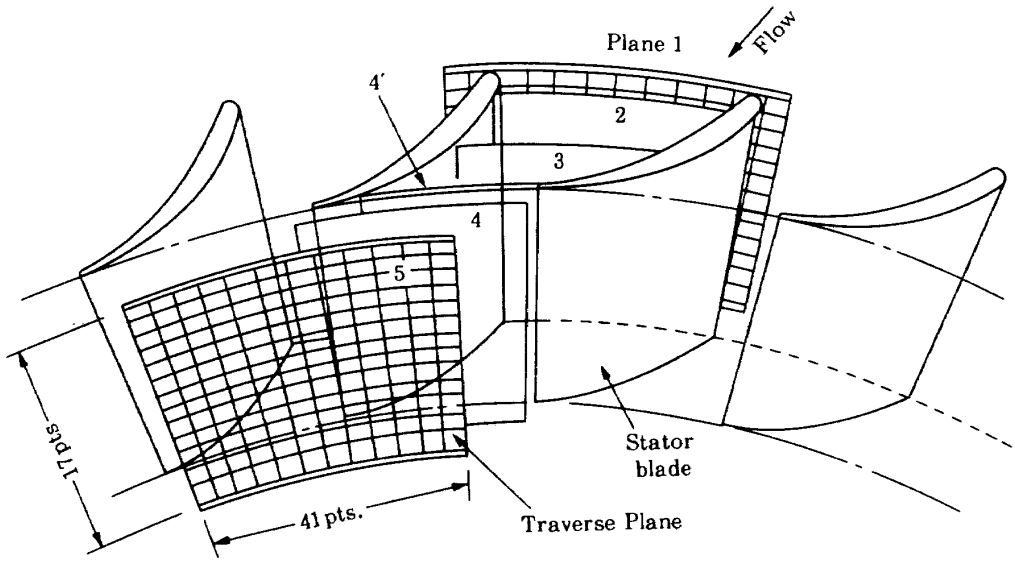

Fig. 2 Traverse measuring planes

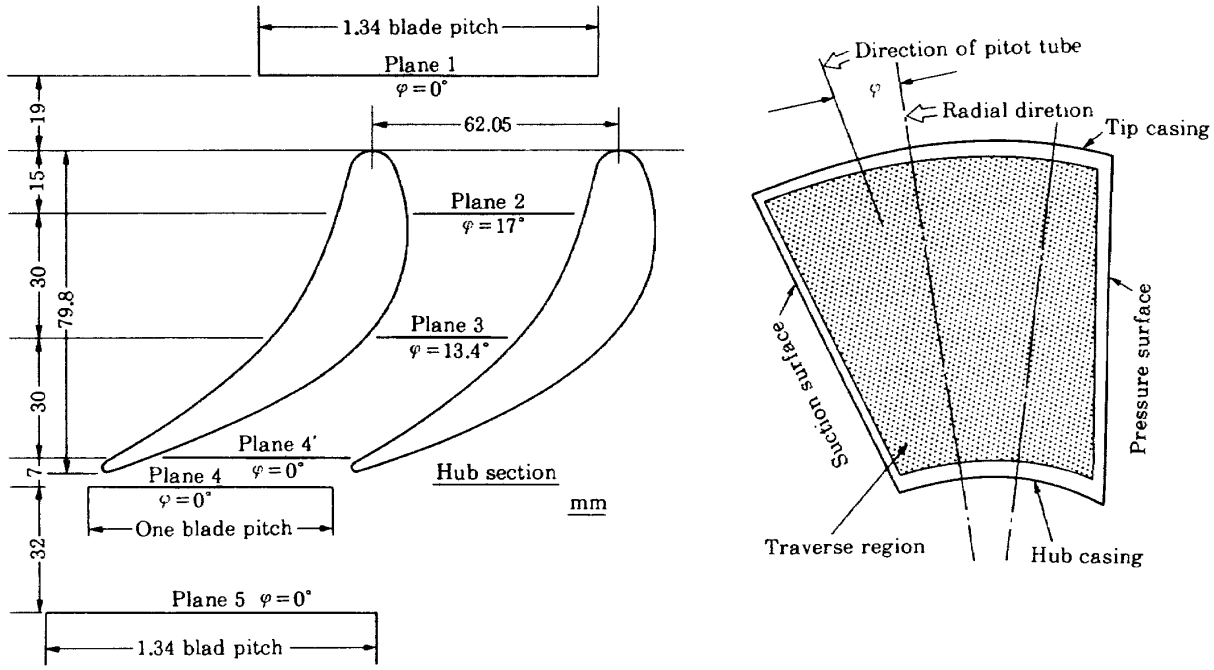

Fig. 3 Axial locations of traverse planes and traverse region within blade row

blade row), 15, 45, 75mm (within the row), 82 and 114mm (downstream the row). They correspond to about -0.24, 0.19, 0.56, 0.94, 1.03 and 1.43 times the axial blade chord. The circumferential traverse widths out of the row are 1.34 x blade-pitch for planes 1 and 5, and one pitch for plane 4.

The sensors used for the present tests are cobra-type five-hole pitot tubes of miniture and ordinary sizes. Their head sizes are 1.5mm for flow measurements at planes 2, 3, 4', 4 and 5, and 3mm at plane 1.

Within the blade row, the area where measurements were made was determined by the ability of the probe to make electrical contact with the blade surfaces and with the hub casing wall. To

be able to traverse the whole flow path, the sensor was installed inclined at an angle (φ) againt the radial direciton of the wind tunnel.

At each of 697 measuring points in each plane, pressures of pitot tubes and other reference pressures were measured by individual pressure transducers to save scanning time (0.6 hour for 7000 bits of pressure data/test). The direction of each sensor was kept fixed during the traverse measurements. The flow angles at each measuring point were determined from the measured pressures with calibrated three dimensional carpets programmed on a VAX 11/750 computer.

Flow visualization tests were made at an inlet velocity of about 1 m/sec ($Re = 8 \times 10^3$) which was different from the velocity used for traverse tests. A single type and a comb type oil-smoke injection pipes of 2.0mm outer diameter (1.6mm inner diameter) were made and installed upstream the cascade. To set the circumferential location of the smoke line relative to a blade and to see the change of flows due to the location, the rotation mechanism of the cascade was also used.

METHOD OF ANALYSIS

Definition of Secondar Flow (Deviation from Mean Flow)

Details of the definition can be found in a previous report [6], in which secondary flows are defined as a set of local flow velocities projected onto a plane which is normal to a mass-averaged yaw direction and parallel to the radial direction. Since the projection plane of secondary flow vectors is parallel to the radial direction, radial components of secondary flows shown later in the results are equal to those of local velocities measured.

Non-dimensional Forms of Total Pressure Loss, Static Pressure and Velocity

The total pressure (Pt) deficit of each plane is expressed in the following dimensionless form:

$$CPt = (\bar{\bar{P}}t,1 - Pt)/(0.5\ \rho\ \bar{\bar{V}}m^2,5)$$

where $\bar{\bar{P}}t,1$ and $\bar{\bar{V}}m,5$ are the mass-averaged inlet total pressure of plane 1 and the outlet velocity of plane 5, respectively.

Similarly, static pressures (Ps) are normalized by

$$CPs = (Ps - \bar{\bar{P}}t,1)/(0.5\ \rho\ \bar{\bar{V}}m^2,5)$$

Velocity (Vm) is expressed as the ratio against the outlet velocity:

$$CVm = Vm/\bar{\bar{V}}m,5$$

The magnitude of the secondary vector (Vs) is also normalized in the same manner.

EXPERIMENTAL RESULTS AND DISCUSSION

Hub Endwall Static Pressure (Fig. 4)

Endwall static pressure measurements were obtained from 108 static pressure holes on the hub endwall. Fig. 4 shows constant contour lines of non-dimensional pressures, where CPw is defined as the ratio of local endwall static pressure minus inlet endwall static pressure far upstream the blade against the inlet dynamic pressure. In front of the blade leading edge, closed contour lines of constant static pressures were found. To keep the periodicity of the cascade flow, some of the contour lines close to the leading edge would be directed onto the blade surface as drawn by dotted lines. The center of the closed lines corresponds to the location of a saddle point where the hub-side horseshoe vortex is formed.

Within the cascade, a flow-decelerating region exists near the suction surface upstream the trailing edge, where flow separation could easily occur. In this region, very complex flows exists, as will be shown later.

Endwall Flow Visualization Near Leading Edge (Fig. 5)

Flow visualization confirmed the saddle point as shown in Fig. 5. A smoke line reaching the

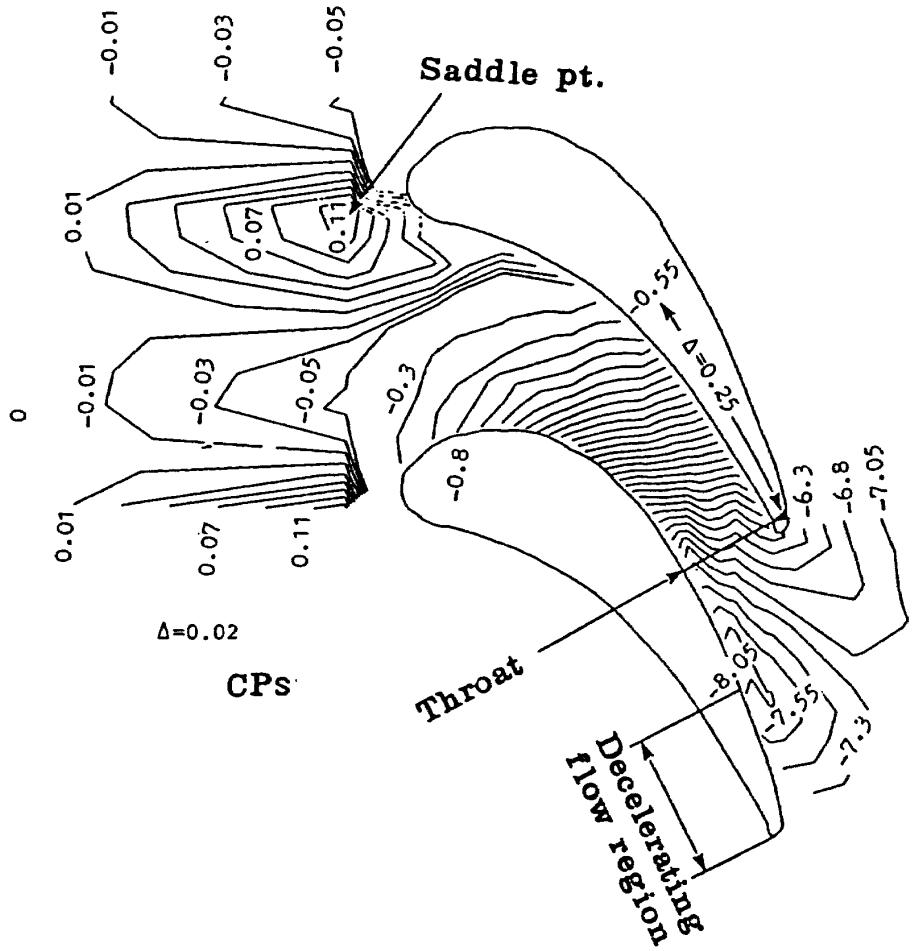

Fig. 4 Hub endwall static pressure

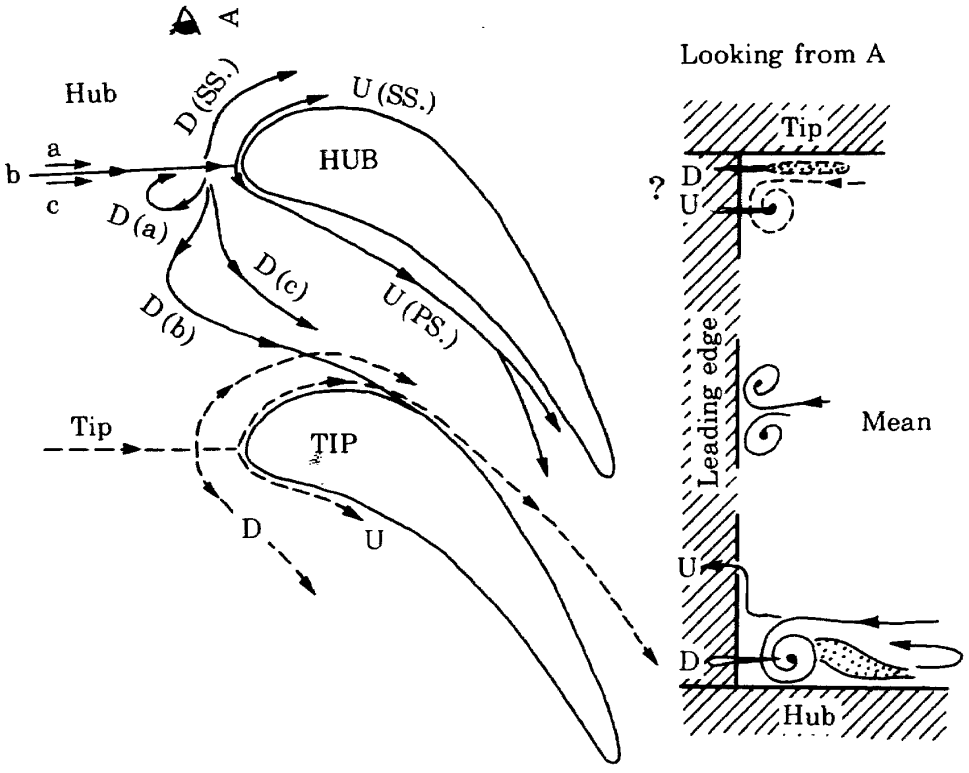

Fig. 5 Endwall flow visualization near leading edge

leading edge at a certain height from the endwall divided into lower and upper flows as shown by D and U. Each flow (D and U) diverged to both sides of the blade. The lower one formed a horse-shoe vortex and the pressure-side leg from the vortex core passed the endwall as shown by lines D (a), (b) and (c). Each direction depends on where the smoke line is located circumferentially on the leading edge. These flow directions agree with those expected from the endwall static pressure distribution. Both of the suction-side flows reached a position of about 1/4 blade height from the hub endwall at the trailing edge. The pressure-side leg of the upper flow passed along the blade pressure surface, keeping some distance from the pressure surface, and divided into two flows downstream within the cascade, as shown in Fig. 5. A similar flow pattern was also recognized within the tip-side endwall flow.

Upstream Flow Field (Plane 1, Fig. 6)

The minimum static pressure appeared near the tip casing between the blades. Following this pressure gradient, secondary flows (deviated flows) passed normal to the constant static pressure contour lines toward the minimum pressure region. The total pressure at the plane was almost uniform.

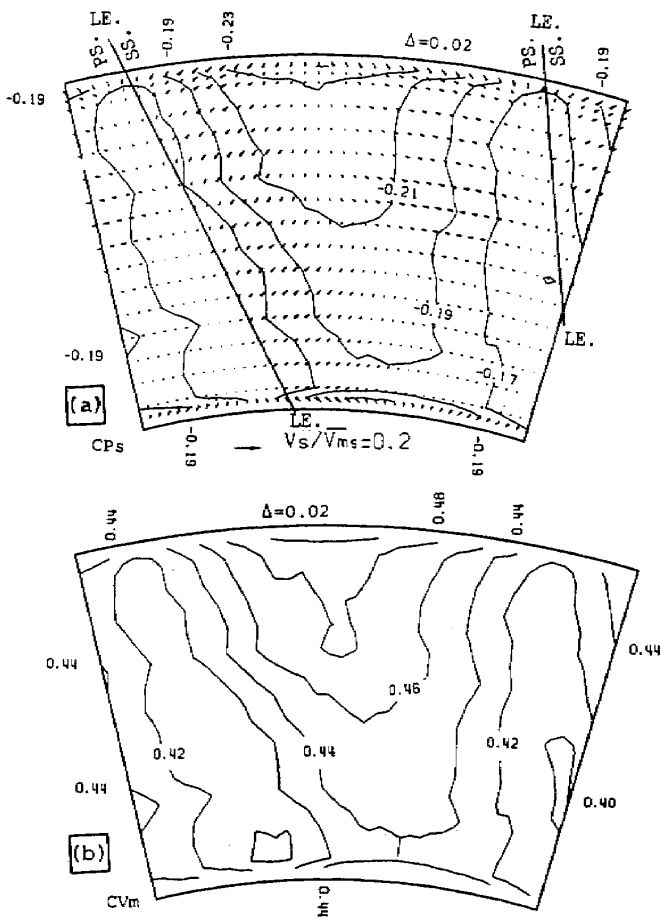

Fig. 6 Upstream flow field (Plane 1)
(a) Static pressure and secondary flow vectors
(b) Velocity

Flow Fields within Blade Row (Planes 2, 3 and 4')

Flow at plane 2 (Fig. 7)

Constant static pressure lines are almost straight from the hub (inner wall) to the tip (outer wall) and almost normal to the hub wall. The span-wise static pressure distribution close to the blade pressure surface is nearly uniform. On the suction surface, however, a large pressure gradient exists in the span-wise direction. At the hub suction surface corner, following this pressure gradient, a boundary layer flow comes from the side of the pressure surface along the hub wall and accumulates a loss in a thickened boundary layer there. In several other tests, where the inlet boundary layer thickness was increased by setting a trip rubber ring of from 0.25 to 1.5 mm height upstream the hub endwall, this local maximum loss region was often not detected in plane 2.

Flow at plane 3 (Fig. 8)

The flow velocity on the suction surface is already greater than the cascade average outlet-flow velocity. In this plane, which is located axially at about a half axial-blade-chord distance from the blade leading edge, strong inward flows toward the hub dominate in the whole flow path, except near the hub endwall. Because the velocity is highest at the tip suction corner, the static pressure is lowest at this corner. Toward the

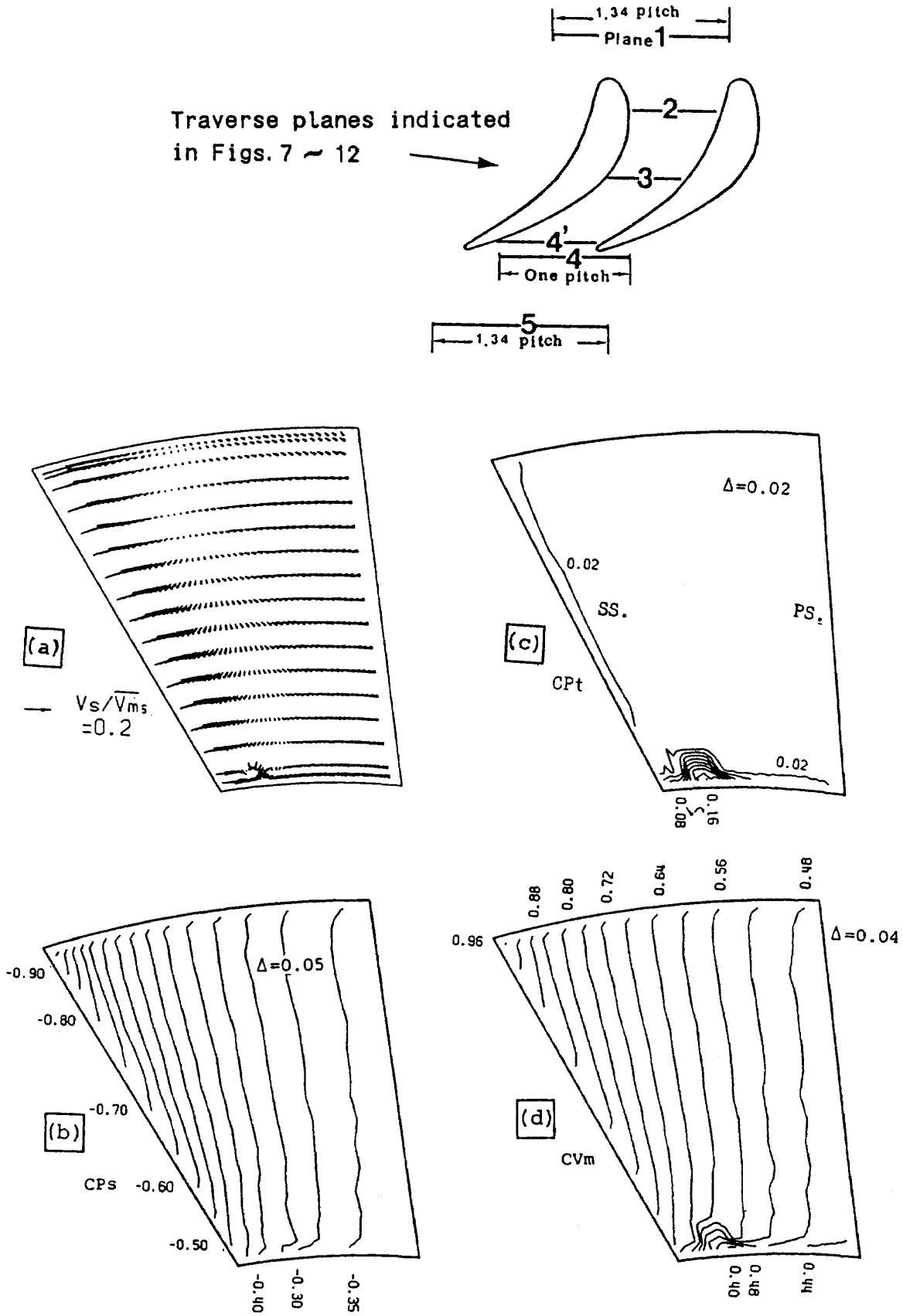

Fig. 7 Flow field within blade row (Plane 2)
(a) Secondary flow vectors, (b) Static pressure
(c) Total pressure loss, (d) Veclocity

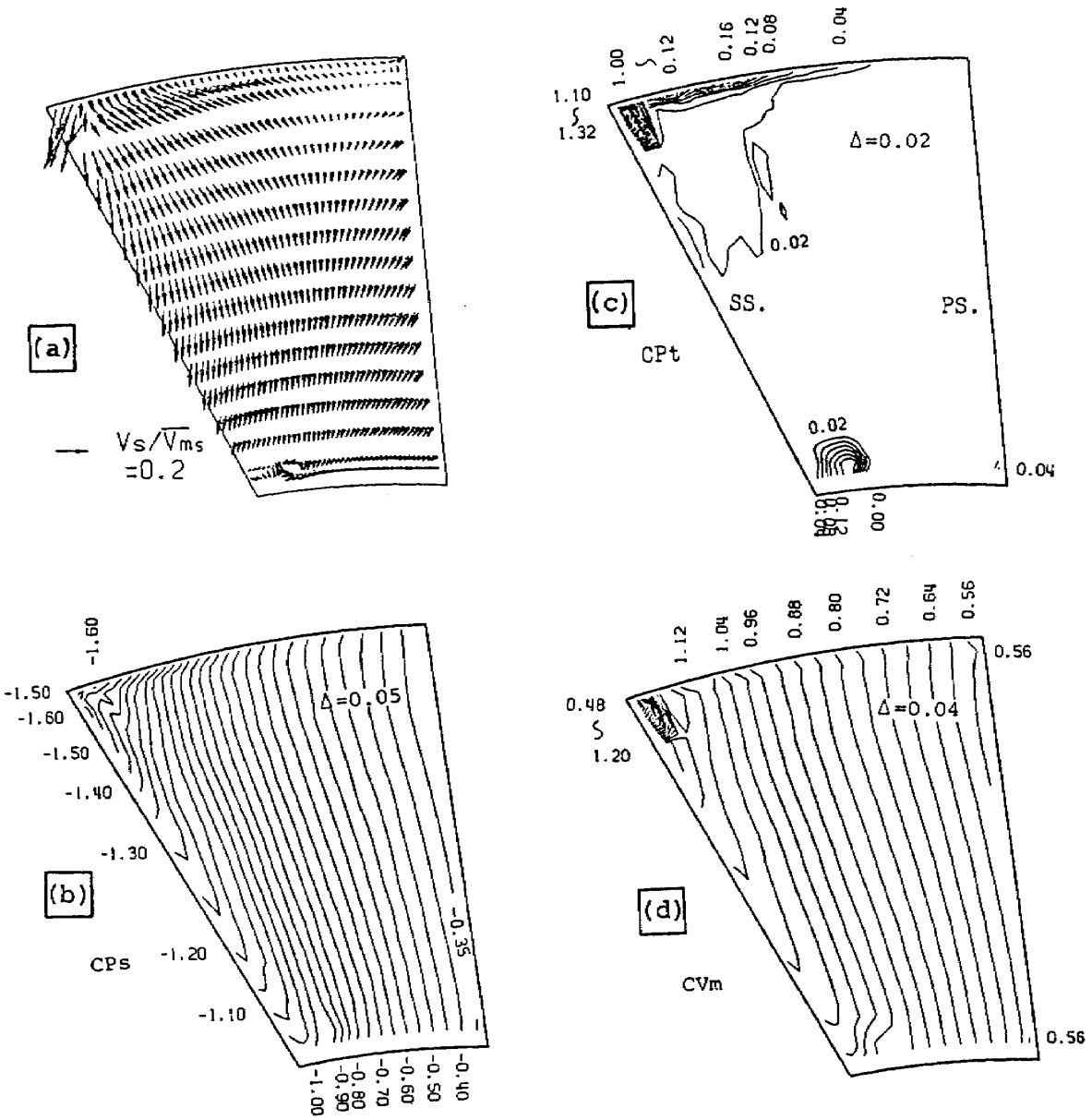

Fig. 8 Flow field within blade row (Plane 3)
(a) Secondary flow vectors, (b) Static pressure
(c) Total pressure loss, (d) Velocity

corner, therefore, low-energy fluids accumulate and form a very high loss region. Velocity there greatly decreases. It is considered that this high loss comes mainly from the tip casing boundary layer and that it starts a surface separation into which the suction surface flow can not pass.

The direction of rotation of secondary flows near the hub suction corner becomes more distinct than before and is clockwise. This suggests that the pressure-side horseshoe vortex or a hub passage vortex rolled up hub boundary layer fluids and formed a loss core at the hub suction corner. In addition to this loss core, a similar loss core was also often seen on the blade suction surface near the corner.

Flow at plane 4′ (Fig. 9)

The results of this plane, located just upstream the trailing edge within the blade row, do not yet include the effects of wake flow.

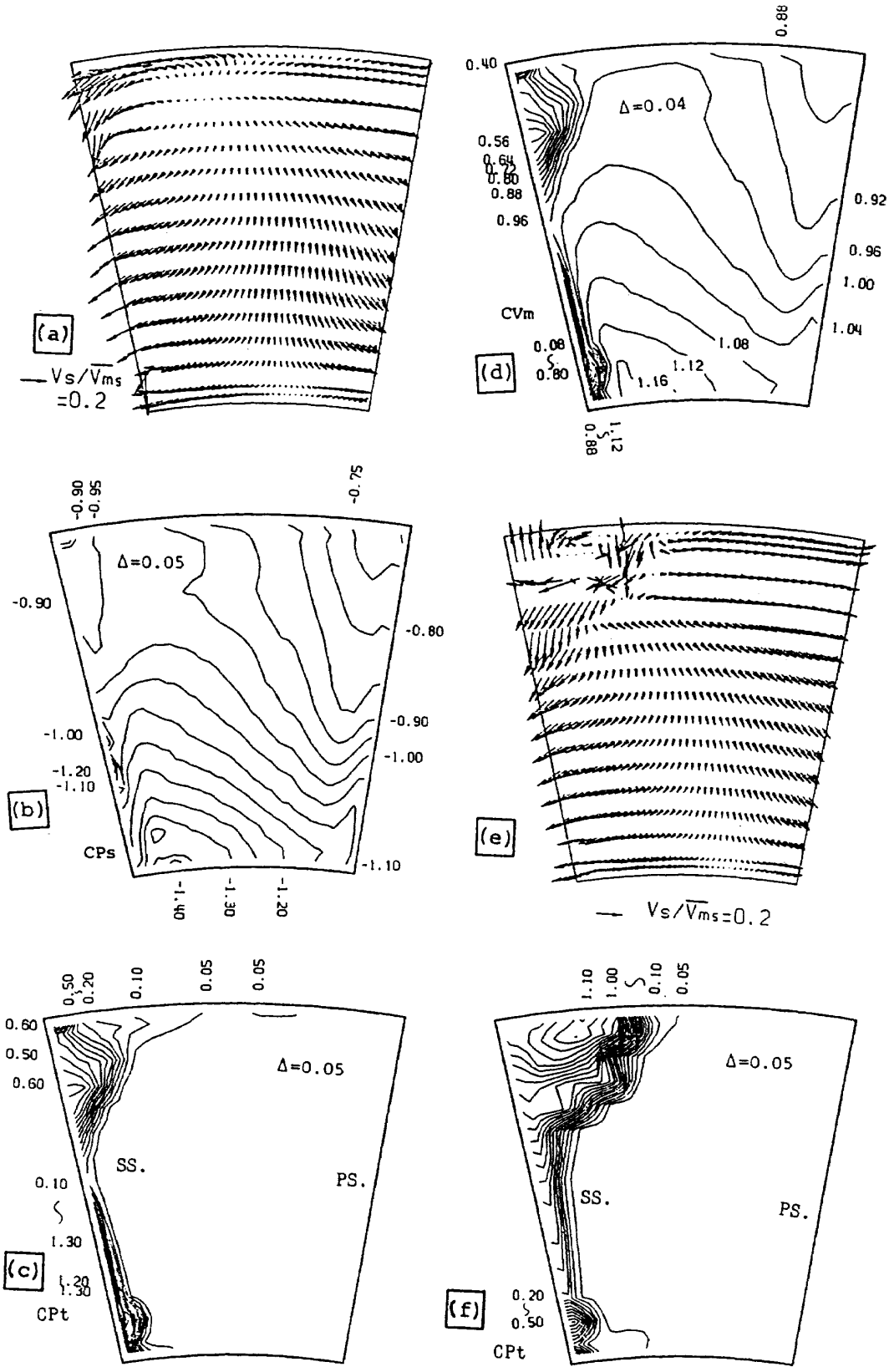

Fig. 9 Flow field within blade row (Plane 4')

(a) (e) Secondary flow vectors, (b) Static pressure

(c) (f) Total pressure loss, (d) Velocity

where (e) and (f) are the case with tip-clearance

The point of highest velocity, which was located at the tip suction surface corner in the previous plane, has moved to the hub in the present plane. Accordingly, the span-wise static pressure gradient on the suction surface is now opposite to that in the previous plane and the low energy fluids accumulated at the tip suction surface corner easily migrate over the suction surface. In other words, forming a clearly recognized passage vortex, low-energy fluids spread out over the suction surface, producing a high-loss core. The low-energy fluids moving toward the hub interact with an outward flow which is a rolling-up hub endwall boundary layer flow. This causes another high loss core at the interaction point. These flow patterns agree with the flow visualization results discussed later.

To show tip clearance effects on the flow fields within the cascade, (which effects are very important in the case of rotor blade rows) Fig. 9 (e and f) are given here. The effects on secondary flows and losses are clearly seen to be very large over the whole blade span. A strong interaction occurs between the leakage flow and the passage vortex.

Downstream Flow Fields (Planes 4 and 5)

Flow at plane 4 (Fig. 10)

Measurements at this plane, just downstream the blade row, include effects of blade wake flow in addition to those obtained at plane 4'. Strong inward wake flows (toward the hub) appear along the trailing edge. The flows also involved flows from the blade pressure side across the wake. The strong inward flows transport low energy fluids to the hub suction corner and interact with the flows rolling up from the hub endwall surface. A dead flow region along the trailing edge is indicated to be deformed in Fig. 10 (d).

Fig. 11 shows another result of boundary layer measurements with finer traverse meshes (0.38 mm × 100 circumferential points × 17 radial points within a half blade-pitch width). As seen in the velocity plot at both sides of the dead flow region, the boundary layer developed on the blade suction surface is thick and not uniform but that on the pressure surface is thin and almost uniform (but not completely uniform, as seen in the figure).

Fig. 10 (e and f) shows the effects of the tip-clearance flow which pushes the tip-side passage vortex toward the hub and increases the pressure loss over the blade suction surface. The strong leakage flow isolates another local maximum loss core on the tip endwall from the suction surface. The leakage flow reduces the cascade outlet yaw angle. The reduced mass-averaged yaw angle in this plane was about 2 degrees in both planes 4' and 4.

Flow at plane 5 (Fig. 12)

The flow field includes two vortices with a counter-clockwise rotation. The outer (tip-side) one corresponds to the shedding vortex of the tip-side passage vortex as seen so far. On the other hand, the inner (hub-side) one is rotating in the opposite direction to that of the hub-side horseshoe or passage vortex which appeared in the previous planes. This inner vortex was, in fact, formed in such a way that the low-energy fluids shedded off from the trailing edge toward the hub and formed a vortex at the hub endwall. Rotation of the vortex in the counter-clockwise direction (i.e., opposite direction to that of the hub passage vortex) is due to the pressure balance near the hub suction-side endwall, as was seen in the figure of static pressure distribution (Fig. 10). This will be seen in the next section, where flow visualization results are described in detail.

Outlet Flow Visualization Near Trailing Edge (Fig. 13)

Fig. 13 shows an overall view of the flow field obtained from streamline trace of smoke and surface streak trace of atomospheric dust. Making a

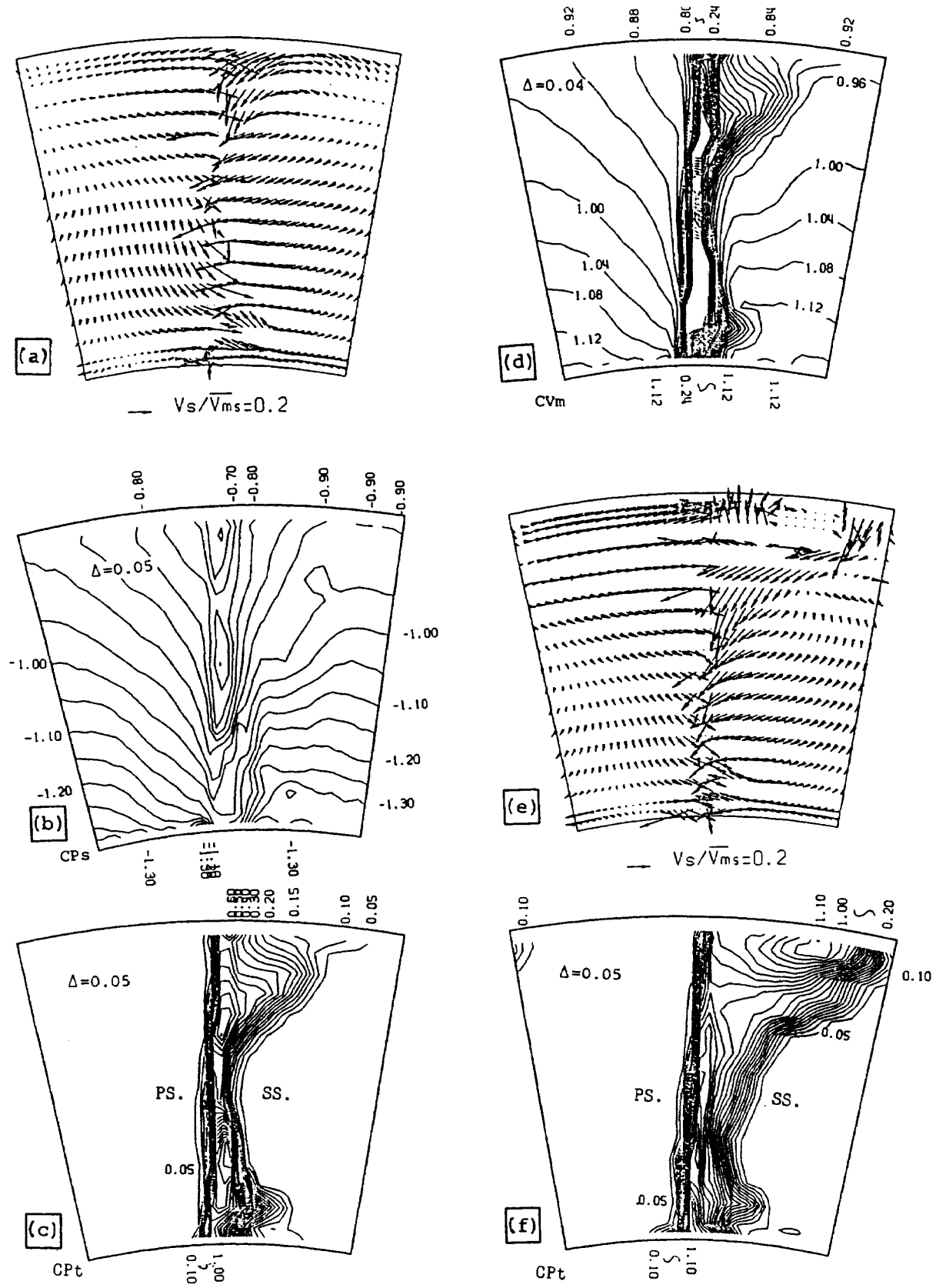

Fig. 10 Downstream flow field (Plane 4)

(a) (e) Secondary flow vectors, (b) Static pressure

(c) (f) Total pressure loss, (d) Velocity

where (e) and (f) are the case with tip-clearance

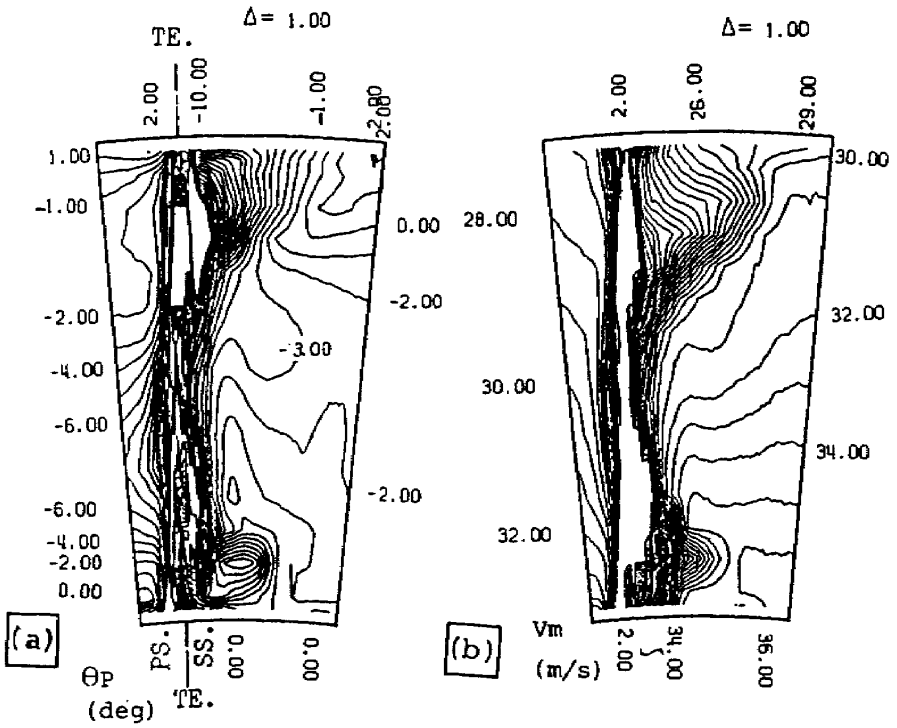

Fig. 11 Boundary layers on both blade surfaces (Plane 4)
(a) Pitch angle, (b) Velocity

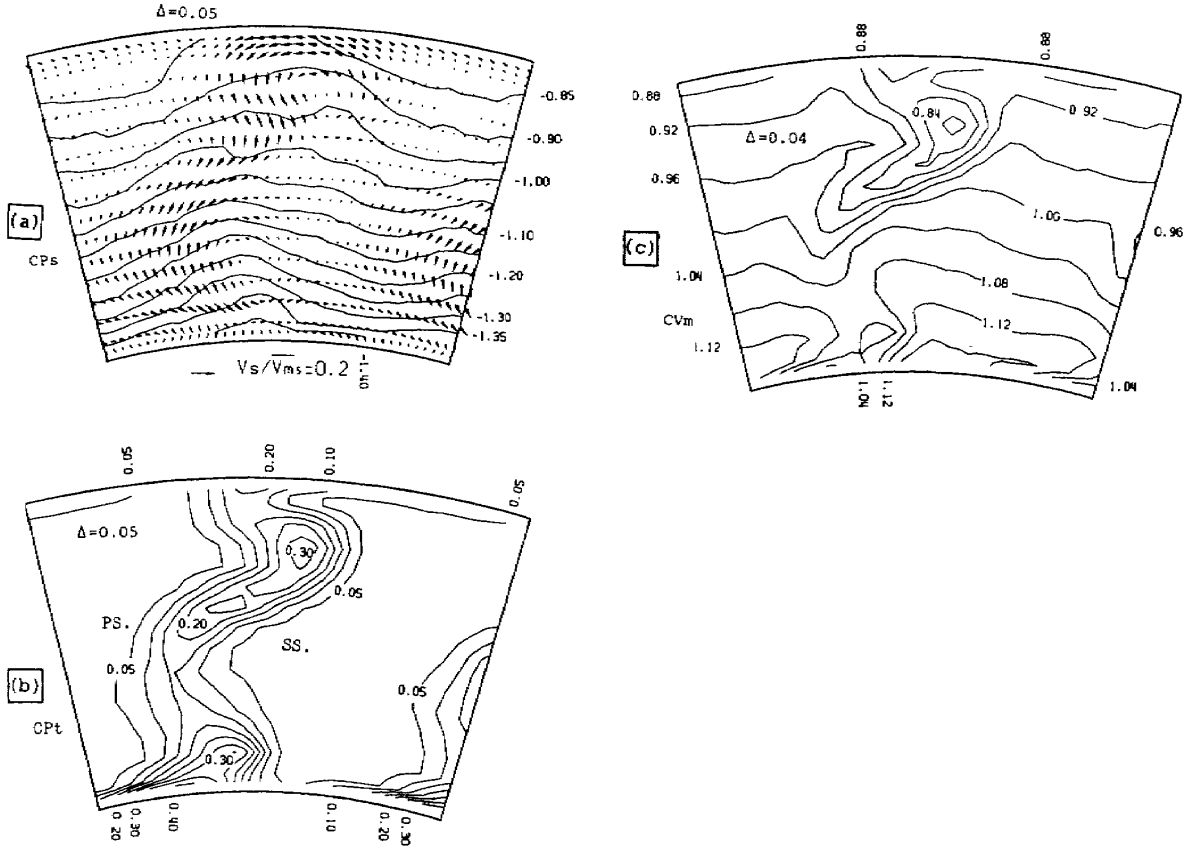

Fig. 12 Downstream flow field (Plane 5)
(a) Static pressure and secondary flow vectors
(b) Total pressure loss, (c) Velocity

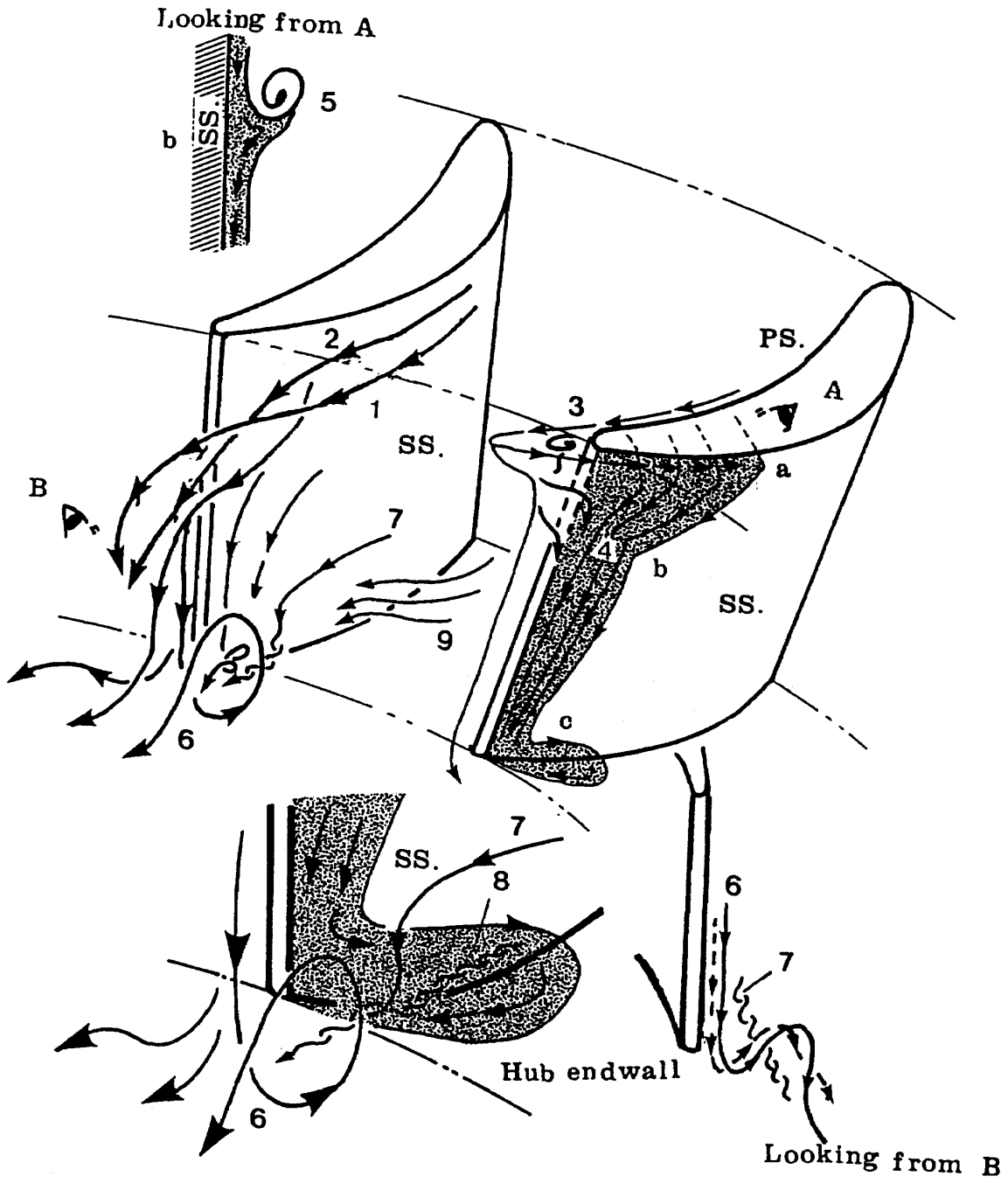

Fig. 13 Outlet flow visualization near trailing edge

1. Flows near tip casing and suction surface
2. Limiting streamline
3. Vortex in the wake and corner b.l. flow around trailing edge
4. Suction surface boundary layer flow
5. Vortex formed at kink b
6. Hub-side shedding vortex formed at hub endwall
7. Suction surface flow being involved into 6
8. Induced vortex tailing from a point on 7
9. Lifted endwall surface flow

a, b, c. Kinks of 4

streamline trace with oil smoke was useful for looking at flows both far from and near the surface, as well as boundary layer flows. After the long runs of the present serial traverse tests, streaks formed by atomospheric dust on the blade surfaces and the endwalls were often visible. Especially on cooled blade surfaces and on hub endwall for static pressure measurements, many streaks originating from small cooling holes and static pressure taps were clearly visible. These suface streaks were also useful for observing surface flow directions.

As shown by 1 in Fig. 13, smoke stream lines near the tip casing rapidly rolled down the suction surface in the hub direction. The streamlines could not enter the space formed at the tip suction-surface corner, as if there were a vacuum at the corner. Flows in the space, however, do not stagnate and have velocities, as was seen in the previous measurements. A part of the boundary layer in the space separates, as will be seen later. This space corresponds to the tip-side high loss region. The boundary of this space, attaching itself to the suction surface, forms a limiting streamline indicated by 2, across which the surface flows can not pass; only the low energy boundary layer flows coming from the tip endwall could.

Close inspection of tip endwall smoke trace revealed that the 'pressure surface' boundary layer along the tip corner entered this region around the trailing edge through the wake, as indicated by 3. Just downstream from the trailing edge near the tip casing, the smoke lines represented a vortical motion moving vertically toward the hub. A part of the low velocity fluids moved upstream along the tip suction corner, following the pressure gradient between the trailing edge and the throat. Then, as indicated by 4, it fell down toward the hub on the surface, similarly to what was reported by Hansen et al. [10]. These flows were clearly seen as a thin smoke film which included very slow velocity fluids. The backward flow in the upstream direction was seen also when blade tip-clearance existed. In this case, a part of the low energy fluids at the pressure surface passed directly across the tip clearance, making a thin smoke film 'on' the blade tip surface (as indicated by dotted lines on the blade tip surface).

The film has three kinks (as indicated by a, b and c) on the blade surface. At point b, a vortex was formed as shown by 5. At point c near the hub suction corner, the boundary layer fluids again flowed back in the upstream direction and fell down to cover a small part of the hub endwall. This behavior could be understood from the endwall pressure gradient.

Another strong vortex was formed as indicated by 6. Flows, shedding from the blade trailing edge at a position closer to the hub than the position of vortex 1, turned very sharply toward the hub along the trailing edge and collided almost normally with the hub endwall. Then this flow rolled up at the suction-side of the trailing edge in the counter-clockwise direction. This strong vortex involved suction surface streamlines flowing into the vortex center, as indicated by 7. Between a certain point on the involved streamline (which is already in rotation) and the hub suction corner boundary layer (seen as a thin smoke film), there exists a small induced vortex, as shown by 8. The vortex seems to be a tail from the streamline and appears to be sucking the low energy fluids from the hub suction surface boundary layer. This vortex corresponds to the hub-side core of *CPt* obtained by the quantitative measurements using pitot tubes, as shown before. Outward streaks of surface streamlines were seen on the suction surface very close to the hub endwall [5].

Summary of Loss Mechanism

Fig. 14 shows color graphics of the total pressure loss at five traverse planes and a schematic drawing showing the loss production process

summalized from the present study. Migration of the boundary layer low-energy fluids onto the blade suction surface occured due to the pressure gradient within the cascade and then the accumulated loss was redistributed due to the trailing edge sheddign vorticies downstream the cascade.

CONCLUSIONS

1. Detailed flow measurements and flow visualization tests were made at six stations before, within and after a low-speed annular turbine stator blade row. A set of complete serial traverse data was presented. An analysis presents many three-dimensional complex flow patterns. Behavior of these flows was reasonably understood from the set of the quantitative and qualitative test results.

2. It was confirmed that, within the cascade, the main part of the loss development process is simply a process of low energy boundary layer fluids migrating from the surrounding walls (both endwalls and blade surfaces) onto the blade suction surface, following the near-surface pressure gradient. The resultant loss profile had two cores in the suction surface non-uniform boundary layer. They were caused mainly by tip-side and hub-side passage vortices.

3. Strong shedding vortices occured downstream from the cascade. The direction of rotation of hub-side shedding vortex was opposite to that expected from the hub-side passage vortex. This vortex affected the upstream flow fields within the cascade in a complex manner through induced vorticities and redistributed the cascade losses.

ACKNOWLEDGEMENTS

The authors wish to thank Mr. T. Torisaki, formerly Deputy Director-General, for his support of the present study, and Mr. H. Tateishi, a staff member of Maruwa Electric Industry for his assistance during a serial test with no blade tip-clearance (NOBL) while he was working as a study assistant for one year (April, 1984-March, 1985). The financial support provided by the Ministry of International Trade and Industry as a part of the national project for development of a high efficiency gas turbine is gratefully acknowledged.

REFERENCES

1. Sjolander, S.A., "The Endwall Boundary Layer in an Annular Cascade of Turbine Nozzle Guide Vanes", Carleton, U., TR ME/A 75-4, Dec. 1975.
2. Bindon, J.P., "The Effect of Hub Inlet Boundary Layer Skewing on the Endwall Shear Flow in an Annular Turbine Cascade", ASME 79-GT-13, 1979.
3. Sieverding, C.H., Van Hove, W., and Boletis, E., "Experimental Study of the Three-Dimensional Flow Field in an Annular Turbine Nozzle Guidevane", ASME 83-GT-120, Dec. 1982.
4. Langston, L.S., Nice, M.L., and Hooper, R.M., "Three-Dimensional Flow within a Turbine Cascade Passage", ASME Journal of Engineering for Power, Vol. 99, No. 1, 1977, pp. 21-28.
5. Yamamoto, A., and Usui, H., "Study of Internal Flows in Cooled Three-Dimensional Blade Rows", Part 1 and 2, Transaction of JSME (in Japanese), Vol. 51, No. 463 (B), 1985, pp. 829-846.
6. Yamamoto, A., and Nouse, H., "Transient Phenomena of Secondary Flows and Losses Downstream a Three-Dimensional Turbine Stator Cascade with/without the Effects of Hub Rotation and of Hub Injection", Symposium on Multi-Dimensional Fluid Transients, ASME Winter Annual Meeting, FED-Vol. 18, Dec. 1984, pp. 51-59.
7. Yamamoto, A., Takahara, K, Nouse, H., Inoue, S., Usui, H., and Mimura, F., "An Aerodynamic Design and the Overall Stage Performance of an Air-Cooled Axial-Flow Turbine",

National Aerospace Laboratory, TR-321T, Jan. 1981 or NASA TT F-16083, 1973.

8. Whitney, W.J., Szanca, E.M., Moffitt, T.P., and Monreo, D.E., "Cold-Air Investigation of a Turbine for High-Temperature-Engine Application, I. Turbine Design and Overall Stator Performance", NASA TN D-3751, 1966.
9. Hansen, A.G., and Herzig, H.Z., and Costello, G.R., "A Visualization Study of Secondary Flows in Cascades", NACA TN 2947, 1953.

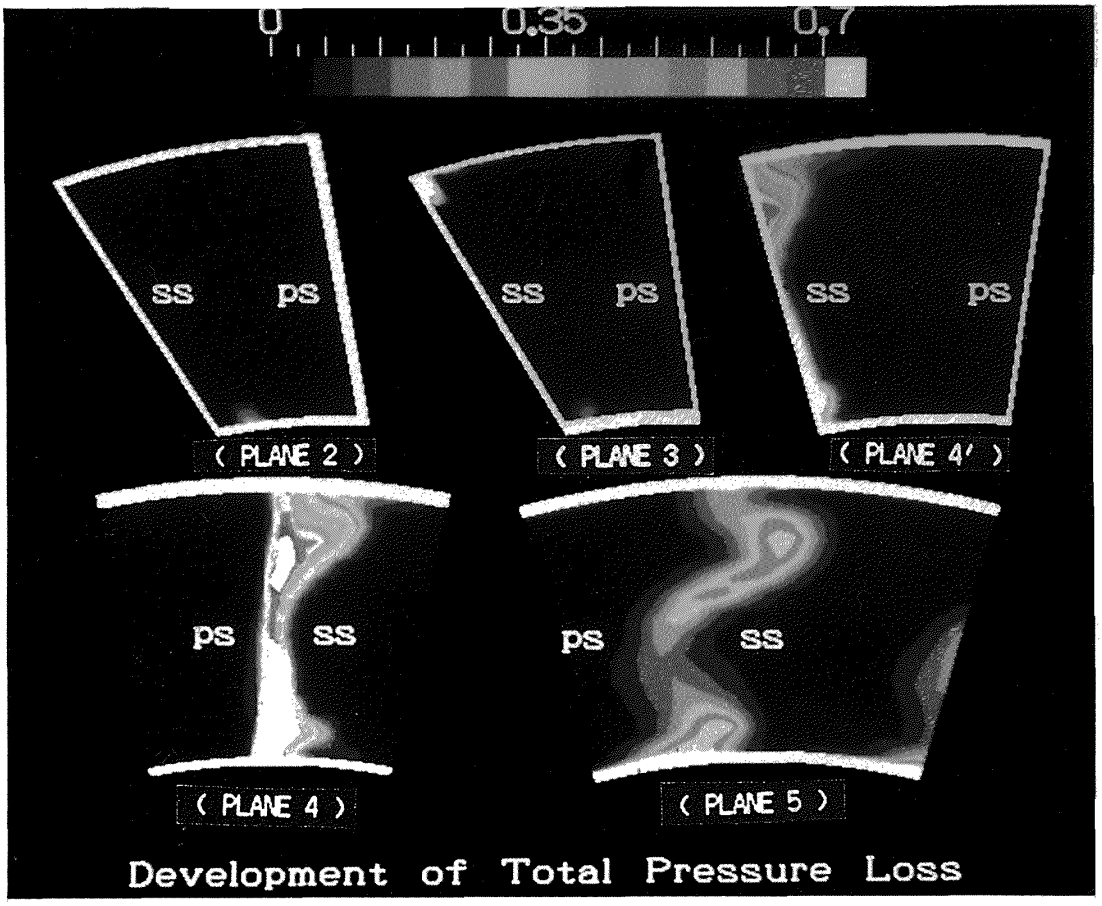

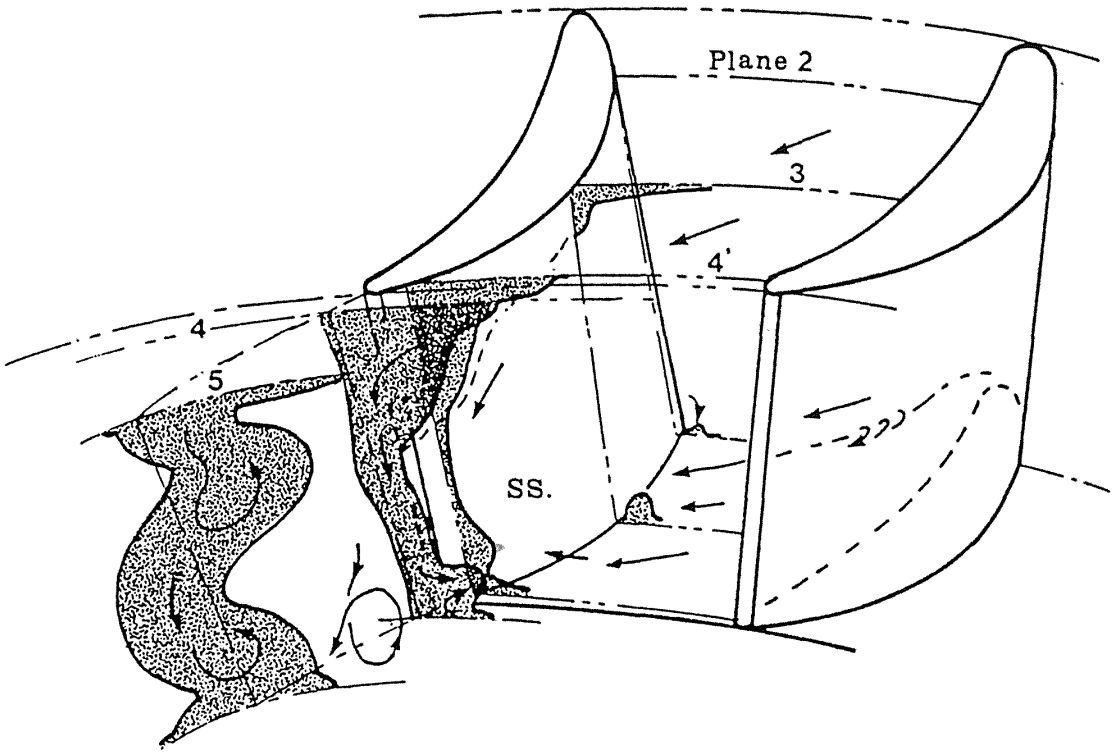

Fig. 14 Cascade loss development process

TECHNICAL REPORT OF NATIONAL
AEROSPACE LABORATORY
TR-970T

航空宇宙技術研究所報告970T号（欧文）

昭和63年4月発行

発行所　航空宇宙技術研究所
東京都調布市深大寺東町7丁目44番地1
電話三鷹(0422) 47-5911（大代表）〒182
印刷所　株式会社　東京プレス
東京都板橋区桜川2－27－12

Published by
NATIONAL AEROSPACE LABORATORY
1,880 Jindaiji, Chōfu, Tokyo
JAPAN

Printed in Japan